C. R. Chimie 14 (2011) 904–910

Contents lists available at ScienceDirect

Comptes Rendus Chimie

www.sciencedirect.com

Full paper/Mémoire

Structural study by X-ray diffraction, magnetic susceptibility and Mössbauer spectroscopy of the $Na_2Mn_{2(1-x)}Cd_{2x}Fe(PO_4)_3$ $(0 \leq x \leq 1)$ solid solution

Mourad Hidouri [a,*], Alain Wattiaux [b], Léopold Fournés [b], Jacques Darriet [b], Mongi B. Amara [a]

[a] UR : matériaux inorganiques, département de chimie, faculté des sciences, 5019 Monastir, Tunisia
[b] Institut de chimie de la matière condensée de Bordeaux, CNRS, 87, avenue du Dr-A.-Schweitzer, 33608 Pessac cedex, France

ARTICLE INFO

Article history:
Received 27 November 2010
Accepted after revision 11 April 2011
Available online 26 May 2011

Keywords:
Phosphate
X-ray diffraction
Magnetic susceptibility
Mössbauer spectroscopy

ABSTRACT

$Na_2Mn_{2(1-x)}Cd_{2x}Fe(PO_4)_3$ $(0 \leq x \leq 1)$ phosphates were prepared by solid state reaction and characterized by powder X-ray diffraction, magnetic susceptibility and Mössbauer spectroscopy. The X-ray diffraction patterns indicated the formation of a continuous solid solution which crystallizes in the alluaudite structural type characterized by the general formula $X(2)X(1)M(1)M(2)_2(PO_4)_3$. The cation distribution, deduced from a structure refinement of the $x = 0$, 0.5 and 1 compositions, is ordered in the $X(2)$ sites and disordered in the remaining $X(1)$, $M(1)$ and $M(2)$ sites. The magnetic susceptibility study revealed an antiferromagnetic behaviour of the studied compounds. The ^{57}Fe Mössbauer spectroscopy confirmed the structural results and proved the exclusive presence of Fe^{3+} ions.

1. Introduction

The term alluaudite designates a large family of mineral phosphates and arsenates either natural or synthetic. The alluaudite type structure was described by Moore who proposed the general formula $X(2)X(1)M(1)M(2)_2(PO_4)_3$ where $X(2)$, $X(1)$, $M(1)$ and $M(2)$ are cationic sites arranged in decreasing size [1]. Its main structural feature is the occurrence of $M(2)_2O_{10}$ dimmers of edge-sharing $M(2)O_6$ octahedra which are alternated by $M(1)O_6$ octahedra that form infinite zig-zag chains in the [1 0 1] direction. These chains are connected by $P(2)O_4$ tetrahedra to form what have been described as "pleated sheets" perpendicular to the [0 1 0] direction. The linkage of these sheets is ensured by the $P(1)O_4$ groups leads to a three-dimensional framework with two sets of tunnels where the $X(2)$ and $X(1)$ sites are located (Fig. 1). The cohesion of the structure is ensured by attractive electrostatic interaction between negative anionic sheets and positive $X(1)$ and $X(2)$ sites. The great flexibility of these sites, demonstrated by their capacity to accommodate a variety of cations with different sizes and charges, leads to the synthesis of a great number of isostructural compounds with different chemical compositions.

As a part of a continuing exploratory study of the A_3PO_4-$M_3(PO_4)_2$-$FePO_4$ systems where A is an alkali metal and M is a divalent cation, we report here the synthesis and structural study, by powder X-ray diffraction, magnetic susceptibility and Mössbauer spectroscopy of the new alluaudite-like solid solution $Na_2Mn_{2(1-x)}Cd_{2x}Fe(PO_4)_3$ $(0 \leq x \leq 1)$.

2. Experimental

Polycrystalline samples of the $Na_2Mn_{2(1-x)}Cd_{2x}Fe(PO_4)_3$ $(0 \leq x \leq 1)$ phosphates were synthesized by conventional solid state reaction starting from stoichiometric mixtures of Na_2CO_3, MnO, $Cd(NO_3)_2{\cdot}4H_2O$, $Fe(NO_3)_3{\cdot}9H_2O$ and $(NH_4)_2HPO_4$. Each of these mixtures was firstly dissolved in diluted nitric acid and the resulting solution was slowly evaporated at 353 K. The dry residue was ground, placed in a platinum crucible and heated in

* Corresponding author.
E-mail address: mourad_hidouri@yahoo.fr (M. Hidouri).

1631-0748/$ – see front matter
doi:10.1016/j.crci.2011.04.002

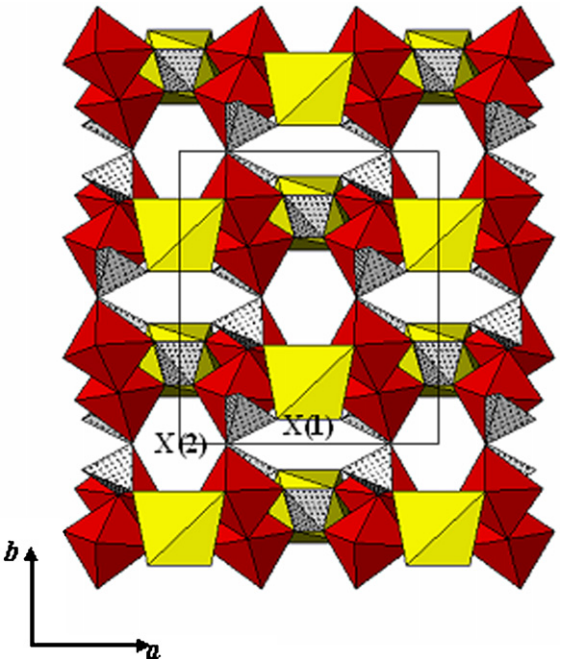

Fig. 1. Polyhedral representation of the alluaudite structure as viewed along the [0 0 1] direction. The M(1)O_6 and M(2)O_6 octahedra are represented by clear and dark polyhydra, and PO_4 by crossed ones.

stages to 473 K, 673 K, 873 K for 24 h at each stage, and to 1173 K for 48 h with intervening grinding. The phase purity of the materials was tested by X-ray powder diffraction. X-ray powder diffraction patterns of the $Na_2Mn_2Fe(PO_4)_3$ ($x = 0$), $Na_2MnCdFe(PO_4)_3$ ($x = 0.5$) and $Na_2Cd_2Fe(PO_4)_3$ ($x = 1$) compositions chosen for the structural refinements were recorded with a Philips PW 1050 diffractometer using graphite monochromatized CuK_α radiation ($\lambda = 1.5406$ Å) and operating in Bragg-Brentano geometry. Refinements were carried out using the Rietveld method [2] and the Fullprof program [3]. The initial atomic coordinates were those of the alluaudite type structure of $Na_{1.79}Mg_{1.79}Fe_{1.21}(PO_4)_3$ [4]. A preliminary examination of the patterns evidenced some additional reflections in that of $Na_2MnCdFe(PO_4)_3$ which indicates small amounts of a secondary phase in the sample. Attempts to identify this phase were unsuccessful. A pseudo-Voigt function was used to describe individual line profiles. The parameters refined include the scale factor, zero point shift, six background parameters, cell parameters and atomic positions. Subsequent refinements of the isotropic thermal displacement parameters (B_{iso}) shown that those of the $X(1)$ and $X(2)$ sites converge to extraordinarily large values which by far exceed those usually obtained in alluaudite-like compounds. Alternative refinements in which these parameters were fixed to the reasonable value 1.0 were undertaken and shown to be successful in view of the resulting R (reliability factors) values. Crystal data and refinement conditions are summarized in Table 1. Final atomic coordinates and thermal displacement parameters are given in Table 2. Observed, calculated and difference profiles are plotted in Fig. 2. The magnetic measurements were done using a Super Conducting Quantum Interference Device (SQUID) MPMS-5S magnetometer. Measurements were carried out at a constant applied magnetic field of 0.5 T in the 2-305 K temperature range. The ^{57}Fe Mössbauer spectra were recorded with a constant acceleration HALDER-type spectrometer using ^{57}Co source (Rh matrix) in the transmission geometry. The polycrystalline absorbers containing about 10 mg.cm^{-2} of iron were used to avoid the experimental widening of the peaks. The velocity was calibrated using pure iron metal as a standard material. All isomer shifts were made in reference to α-Fe.

Table 1
Main crystal data for the $Na_2Mn_{2(1-x)}Cd_{2x}Fe_{1+x}(PO_4)_3$ ($x = 0$; 0.5; 1) compositions.

	$Na_2Mn_2Fe(PO_4)_3$	$Na_2MnCdFe(PO_4)_3$	$Na_2Cd_2Fe(PO_4)_3$
Space group	C2/c	C2/c	C2/c
Formula units/cell (Z)	4	4	4
a (Å)	12.039(3)	12.169(4)	12.297(4)
b (Å)	12.625(3)	12.692(4)	12.799(4)
c (Å)	6.511(2)	6.530(2)	6.562(2)
β (°)	114.54(2)	114.56(2)	114.85(2)
Volume	900.21(4)	917.58(5)	937.06(2)
Temperature (K)	298	298	298
Angular range	($10° \leq 2\theta \leq 120°$)	($10° \leq 2\theta \leq 120°$)	($10° \leq 2\theta \leq 120°$)
Step scan increment	0.02°	0.02°	0.02°
Zeropoint (2θ)	0.022(2)	−0.015(2)	0.019(2)
Pseudo-Voigt function			
$[PV = \eta L + (1-\eta)G]$	η = 0.40(2)	η = 0.47(3)	η = 0.43(3)
No. of refined parameters	56	56	59
Asymmetry parameter	0.03(1)°	0.06(1)	0.06(1)
Pref. orientation parameter	0.99(1)	0.97(4)	0.99(2)
R_p	0.11	0.13	0.09
R_{wp}	0.15	0.16	0.13
R_{exp}	0.12	0.11	0.10
χ^2	1.5	2.0	1.7
R_B	0.06	0.09	0.07
R_F	0.04	0.06	0.04

3. Results

3.1. X-ray diffraction

The X-ray diffraction patterns of the $Na_2Mn_{2(1-x)}Cd_{2x}Fe(PO_4)_3$ compounds are close to that of the alluaudite indicating the formation of a continuous solid solution with the same structure type. The cell parameters a, b, c and β as well as the cell volume V are found to increase with increasing Cd content, in accordance with a larger ionic radius of Cd^{2+} (r_i = 0.95 Å) compared to that of Mn^{2+} (r_i = 0.80 Å) for an octahedral environment [5]. The identification and quantification of the cation distribution in the alluaudite type structures is usually not a straightforward task because the *X*(2), *X*(1), *M*(1) and *M*(2) sites are known to be so flexible that they can accommodate a variety of cations with different sizes and charges. Moreover, the *X*(1) and *X*(2) sites can be occupied or left vacant with no significant effect on the structure [1,6]. For the title solid solution, several distributions were envisaged. They include a totally ordered distribution, an ordered distribution in some sites and disorder in the others, and a totally disordered distribution. The best agreements between the calculated and observed patterns resulting in reasonable *R* values were obtained for the distribution specified in Table 2. In terms of the general formula of the alluaudite, this distribution is given by $[(Na)^{X(2)}][(Na_{0.8}M_{0.2})^{X(1)}][Na_{0.2}M_{0.8})^{M(1)}][(M_{0.5}Fe_{0.5})^{M(2)}]_2(PO_4)_3$. It shows that the title solid solution is formed by cationic substitutions of Mn^{2+} to Cd^{2+} according to: $Mn^{2+} \rightarrow Cd^{2+}$. These substitutions occurred in the *M(2)* sites. Main interatomic distances and angles are listed in Table 3. The *X*(2) site is fully occupied by Na^+ ions. As often occurs for alkali ions, the environment of this site exhibits a wide range of bond lengths and it is difficult to separate bonding and non-bonding contacts. One of the simplest criteria is to consider all distances which are shorter than the shortest Na^+ to next cation. The *X*(2) environment then consists of eight oxygen atoms which form a gable disphenoid similar

Table 2
Atomic coordinates and isotropic thermal displacement parameters for $Na_2Mn_{2(1-x)}Cd_{2x}Fe_{1+x}(PO_4)_3$ (x = 0; 0.5; 1).

$Na_2Mn_2Fe(PO_4)_3$					
Site	Atom	*x*	*y*	*z*	B(Å^2)
X(2)	Na	0	0.019(2)	3/4	1.0
X(1)	0.8 Na + 0.2 Mn	1/2	0	0	1.0
M(1)	0.8 Mn + 0.2 Na	0	0.269(1)	1/4	0.5(1)
M(2)	0.5 Fe + 0.5 Mn	0.221(2)	0.155(1)	0.139(1)	0.3(1)
P(1)	P	0	0.286(1)	3/4	0.4(2)
P(2)	P	0.237(1)	−0.106(1)	0.130(1)	1.0(2)
O(11)	O	0.043(1)	0.211(1)	0.961(2)	1.0(2)
O(12)	O	0.095(1)	0.363(1)	0.737(2)	1.0(2)
O(21)	O	0.372(1)	−0.092(1)	0.172(2)	1.0(2)
O(22)	O	0.172(1)	−0.001(1)	0.119(2)	1.0(2)
O(23)	O	0.163(1)	−0.160(1)	0.896(2)	1.0(2)
O(24)	O	0.225(1)	−0.174(1)	0.317(2)	1.0(2)
$Na_2MnCdFe(PO_4)_3$					
Site	Atom	*x*	*y*	*z*	B(Å^2)
X(2)	Na	0	0.022(2)	3/4	1.0
X(1)	0.8 Na + 0.2 Cd	1/2	0	0	1.0
M(1)	0.8 Cd + 0.2 Na	0	0.269(1)	1/4	0.8(1)
M(2)	0.5 Fe + 0.5 Mn	0.224(1)	0.154(1)	0.141(1)	0.5(1)
P(1)	P	0	0.277(1)	3/4	0.5(2)
P(2)	P	0.234(1)	−0.105(1)	0.136(1)	0.5(2)
O(11)	O	0.053(1)	0.202(1)	0.965(2)	0.7(2)
O(12)	O	0.102(1)	0.354(1)	0.745(2)	0.7(2)
O(21)	O	0.365(1)	−0.080(1)	0.172(2)	0.7(2)
O(22)	O	0.172(1)	0.002(1)	0.116(2)	0.7(2)
O(23)	O	0.173(1)	−0.155(1)	0.912(2)	0.7(2)
O(24)	O	0.221(1)	−0.172(1)	0.312(2)	0.7(2)
$Na_2Cd_2Fe(PO_4)_3$					
Site	Atom	*x*	*y*	*z*	B(Å^2)
X(2)	Na	0	0.023(2)	3/4	1.0
X(1)	0.8 Na + 0.2 Cd	1/2	0	0	1.0
M(1)	0.2 Na + 0.8 Cd	0	0.270(1)	1/4	0.4(1)
M(2)	0.5 Fe + 0.5 Cd	0.226(1)	0.152(1)	0.147(1)	0.5(1)
P(1)	P	0	0.282(1)	3/4	0.5(2)
P(2)	P	0.236(1)	−0.104(1)	0.134(1)	0.5(2)
O(11)	O	0.046(1)	0.206(1)	0.958(2)	0.7(2)
O(12)	O	0.093(1)	0.359(1)	0.734(2)	0.7(2)
O(21)	O	0.366(1)	−0.085(1)	0.174(2)	0.7(2)
O(22)	O	0.172(1)	−0.001(1)	0.119(2)	0.7(2)
O(23)	O	0.165(1)	−0.158(1)	0.906(2)	0.7(2)
O(24)	O	0.228(1)	−0.168(1)	0.316(2)	0.7(2)

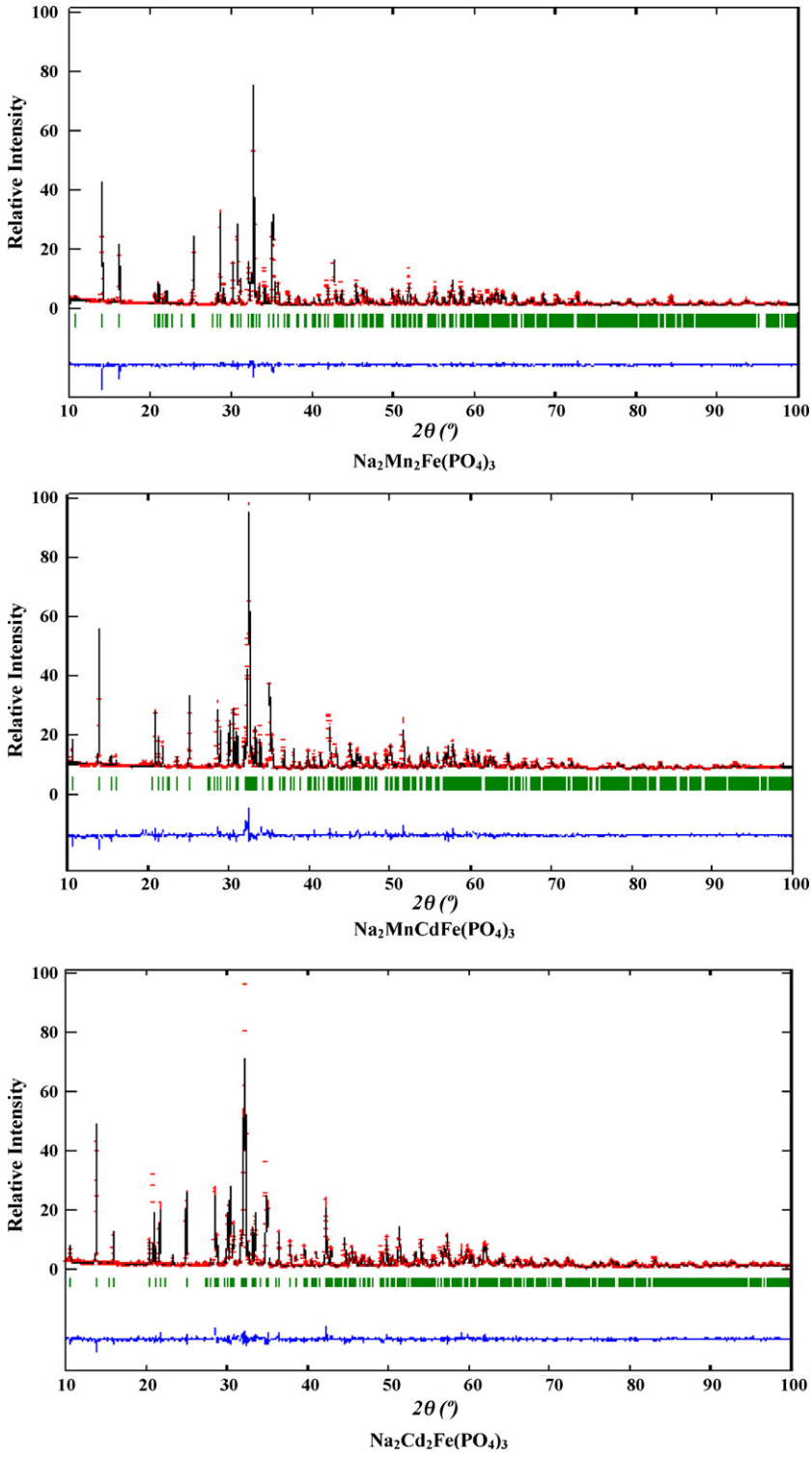

Fig. 2. Observed (crosses), calculated (full lines) and difference (bottom) X-ray powder diffraction patterns for the $Na_2Mn_{2(1-x)}Cd_{2x}Fe_{1+x}(PO_4)_3$ ($x = 0$; 0.5; 1) compounds.

to that observed in $Na_4CaFe_4(PO_4)_6$ [7]. Contrary to $X(2)$, the $X(1)$ site features a statistical distribution of Na^+ and M^{2+} (M = Mn or Cd) in an atomic ratio of approximately 4:1. Considering the same criteria used for $X(2)$, this site is also surrounded by eight oxygen atoms which form a highly distorted cube. The $M(1)$ site is occupied by Mn^{2+} and Cd^{2+} while that of the $M(2)$ type contains a disordered distribution of Fe^{3+}, Mn^{2+} and Cd^{2+}. The contents of the Fe^{3+} and

Table 3
Main interatomic distances in $Na_2Mn_{2(1-x)}Cd_{2x}Fe_{1+x}(PO_4)_3$ ($x = 0$; 0.5; 1).

	$Na_2Mn_2Fe(PO_4)_3$	$Na_2MnCdFe(PO_4)_3$	$Na_2Cd_2Fe(PO_4)_3$
M(1)-O(11) × 2	2.271(1)	2.371(2)	2.361(2)
M(1)-O(21) × 2	2.234(1)	2.425(2)	2.385(2)
M(1)-O(23) × 2	2.264(1)	2.403(2)	2.341(2)
<M(1)-O>	**2.256**	**2.399**	**2.362**
M(2)-O(11)	2.091(1)	2.005(2)	2.150(2)
M(2)-O(12)	2.023(1)	1.930(2)	2.014(2)
M(2)-O(22)	2.004(1)	2.035(2)	2.042(2)
M(2)-O(23)	2.063(1)	2.106(2)	2.132(2)
M(2)-O(24)	2.126(1)	2.135(2)	2.190(2)
M(2)-O(24)'	2.217(1)	2.272(2)	2.345(2)
<**M(2)-O**>	**2.087**	**2.080**	**2.145**
P(1)-O(11) × 2	1.566(1)	1.600(2)	1.578(2)
P(1)-O(12) × 2	1.532(1)	1.588(2)	1.550(2)
<**P(1)-O**>	**1.549**	**1.594**	**1.564**
P(2)-O(21)	1.539(1)	1.549(2)	1.526(2)
P(2)-O(22)	1.553(1)	1.535(2)	1.538(2)
P(2)-O(23)	1.565(1)	1.486(2)	1.544(2)
P(2)-O(24)	1.547(1)	1.500(2)	1.489(2)
<**P(2)-O**>	**1.551**	**1.518**	**1.524**
X(1)-O(12) × 2	2.281(1)	2.420(2)	2.331(2)
X(1)-O(21) × 2	2.359(1)	2.324(2)	2.345(2)
X(1)-O(21)' × 2	2.537(2)	2.547(2)	2.604(2)
X(1)-O(12)' × 2	2.979(2)	3.123(2)	3.049(2)
<**X(1)-O**>	**2.539**	**2.590**	**2.582**
X(2)-O(11) × 2	2.740(2)	2.608(2)	2.651(2)
X(2)-O(22) × 2	2.433(1)	2.453(2)	2.478(2)
X(2)-O(22)' × 2	2.608(1)	2.599(2)	2.617(2)
X(2)-O(23) × 2	2.893(2)	2.961(2)	2.976(2)
<**X(2)-O**>	**2.668**	**2.655**	**2.680**

Table 4
Magnetic properties for $Na_2Mn_{2(1-x)}Cd_{2x}Fe_{1+x}(PO_4)_3$ ($x = 0$; 0.5; 1).

Compound	$Na_2Mn_2Fe(PO_4)_3$	$Na_2MnCdFe(PO_4)_3$	$Na_2Cd_2Fe(PO_4)_3$
Behaviour	Antiferromagnetic	Antiferromagnetic	Antiferromagnetic
T_N (K)	17	15	12
C (emu.mol^{-1}.K)	4.14	4.42	4.40
μ_{eff} (μ_B)	5.76	5.95	5.93

Mn^{2+} ions within the *M(2)* site were fixed to their theoretical values since these ions cannot be distinguished by X-ray Rietveld refinement. As suggested by the *M*(1)-O and *M*(2)-O bond lengths, the octahedral geometry of these sites is strongly distorted. Similar deformation is common in the alluaudite-like structures and it is in part due to the edge-sharing between the $M(1)O_6$ and $M(2)O_6$ octahedra. The two crystallographically distinct PO_4 contained in the structure have P-O bond lengths in the range 1.489(2)–1.600(2) Å. Their overall average of 1.550 Å is comparable to those frequently reported for anhydrous monophosphates.

3.2. Magnetic susceptibility

The temperature dependencies of the inverse molar magnetic susceptibility χ^{-1} for the $Na_2Mn_{2(1-x)}Cd_{2x}Fe(PO_4)_3$ ($x = 0$, 0.5, 1) compounds are illustrated in Fig. 3 and the magnetic characteristics are summarized

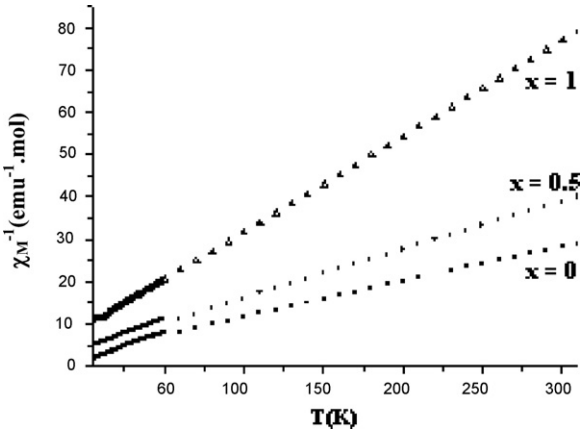

Fig. 3. The inverse molar magnetic susceptibility x^{-1} as function of temperature for the $Na_2Mn_{2(1-x)}Cd_{2x}Fe(PO_4)_3$ ($x = 0$; 0.5; 1) compounds.

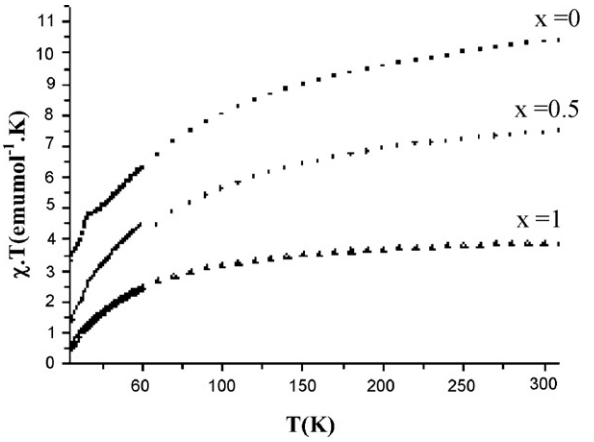

Fig. 4. Thermal variation of the χ.T product for $Na_2Mn_{2(1-x)}Cd_{2x}Fe(PO_4)_3$ ($x = 0$; 0.5; 1).

in Table 4. The curves are similar and they indicate a transition from paramagnetic to antiferromagnetic state at $T_N = 17(1)$, 15(1) and 12(1) K for $x = 0$, 0.5 and 1, respectively. Above T_N, the Curie-Weiss law is obeyed. The Curie constant and the effective magnetic moment are in accordance with the theoretical spin only values for high spin Mn^{2+}/Fe^{3+} ions ($C = 4.375$ emu.mol^{-1}.K and $\mu = 5.92\ \mu_B$). The Curie temperature θ_P, determined through a linear least squares extrapolation to zero is negative indicating that the exchange interactions which occur at low temperatures are predominantly antiferromagnetic. The θ_P values and subsequently the magnetic interactions are decreased when the paramagnetic Mn^{2+} ions are substituted by the diamagnetic Cd^{2+} ones. The antiferromagnetic character of the title solid solution is supported by the plots of the χ.T products (Fig. 4) which decrease with decreasing temperature. However, a careful examination of the plot for $Na_2Mn_2Fe(PO_4)_3$ shows a significant increase of the χ.T product at the Néel temperature. A similar behaviour has already been observed for the phosphates $Ag_2Mn_2Fe(PO_4)_3$ [8] and $KMn_4(PO_4)_3$ [9] and it was attributed to a possible magnetic phase transition occurring at critical temperature.

3.3. Mössbauer spectroscopy

The room temperature Mössbauer spectra for the $Na_2Mn_{2(1-x)}Cd_{2x}Fe(PO_4)_3$ ($x = 0$, 0.5, 1) compounds are shown in Fig. 5. They exhibit two resonance absorption lines with large line widths, resulting from a superposition

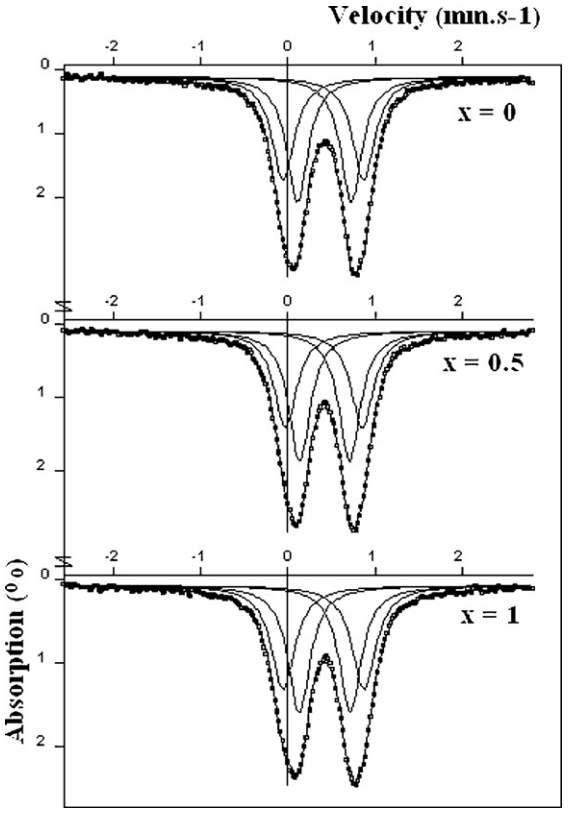

Fig. 5. The Mössbauer spectra of $Na_2Mn_{2(1-x)}Cd_{2x}Fe_{1+x}(PO_4)_3$ ($x = 0$; 0.5; 1) at 293 K.

of many iron site environments. The spectra were refined using lorantzian profile lines and the best results were obtained by considering two doublets assigned to two different iron sites. The hyperfine parameters deduced from the refinements are given are in Table 5. The isomer shifts ($0.42(2)$ mm/s $< \delta < 0.44(2)$ mm/s) are close to those usually observed for Fe^{3+} in octahedral environment [10]. According to the structure refinements, iron occupies statistically 50% of the $M(2)$ sites and the remaining 50% of the sites are occupied by a distribution of M^{2+} cations (M = Mn or Cd). The iron environments within the $M(2)_2O_{10}$ dimmers are then split in two types, namely Fe_2O_{10} and (Fe, M)$_2O_{10}$ and which have the same probability of existence. Effectively, the Mössbauer spectroscopy shows two iron sites Fe(1) and Fe(2) with very similar isomer shifts and quasi-identical populations. From a comparison of the quadrupole splitting values for Fe(1)

Table 5
Mössbauer spectral parameters for $Na_2Mn_{2(1-x)}Cd_{2x}Fe_{1+x}(PO_4)_3$ ($x = 0$; 0.5; 1).

Compound	Site	δ (mm.s^{-1})	$<\Delta>$ (mm.s^{-1})	Γ (mm.s^{-1})	% population
$Na_2Mn_2Fe(PO_4)_3$	*Fe(1)*	0.420(10)	0.925(10)	0.311(8)	46.5
	Fe(2)	0.430(8)	0.619(8)	0.295(6)	53.5
$Na_2MnCdFe(PO_4)_3$	*Fe(1)*	0.425(10)	0.885(10)	0.317(9)	44.10
	Fe(2)	0.433(7)	0.574(7)	0.298(6)	55.90
$Na_2Cd_2Fe(PO_4)_3$	*Fe(1)*	0.421(9)	0.931(9)	0.331(9)	47.00
	Fe(2)	0.434(7)	0.587(7)	0.304(6)	53.00

and Fe(2), one can deduce that the Fe(2) environment ($\Delta EQ_2 = 0.60(1)\ mm.s^{-1}$) is more regular than that of Fe(1) ($\Delta EQ_1 = 0.90(1)\ mm.s^{-1}$). Thus, the Fe(2) site can be attributed to the Fe_2O_{10} type environment and the Fe(1) to that of (Fe, M)$_2O_{10}$ type. The strong distortion of the latter environment is due to the difference between the ionic radii of the M^{2+} and Fe^{3+} ions.

4. Conclusion

A new solid solution $Na_2Mn_{2(1-x)}Cd_{2x}Fe(PO_4)_3$ ($0 \leq x \leq 1$) has been prepared and shown to be of the alluaudite type. According to the $X(2)X(1)M(1)M(2)_2(PO_4)_3$ general formula of the alluaudite structure, the cation distribution can be summarized by: $[(Na)^{X(2)}]$ $[(Na_{0.8}M_{0.2})^{X(1)}]$ $[Na_{0.2}M_{0.8})^{M(1)}][(M_{0.5}Fe_{0.5})^{M(2)}]_2(PO_4)_3$ where M is Mn or Cd. This solid solution is then formed by cationic substitutions within the *M(2)* sites according to: $Mn^{2+} \rightarrow Cd^{2+}$. Magnetic susceptibility measurements indicated an antiferromagnetic behaviour of the studied compounds with Néel temperatures of 17(1), 15(1) and 12(1) K, for $x = 0$, 0.5 and 1, respectively. The Mössbauer spectroscopy results were consistent with the structures and confirmed exclusive presence of octahedral Fe^{3+} ions.

References

[1] P.B. Moore, Am. Mineral 56 (1971) 1955.
[2] H.M. Rietveld, Acta Crystallogr. 22 (1967) 151.
[3] J. Rodriguez-Carvajal, Fullprof version 1.9c, mai 2001, LLB.
[4] M. Hidouri, B. Lajmi, A. Driss, M.B. Amara, Acta Crystallogr. E59 (2003) i7.
[5] R.D. Shannon, Acta Crystallogr. 32 (1976) 751.
[6] D. Antneucci, G. Miehe, P. Tarte, W.W. Schmahal, A.M. Fransolet, Eur. J. Mineral 5 (1993) 207.
[7] M. Hidouri, B. Lajmi, A. Wattiaux, L. Fournés, J. Darriet, M.B. Amara, J. Solid State Chem. 177 (2004) 55.
[8] N. Chouaibi, A. Daidouh, C. Pico, A. Strantrich, M.L. Veiga, J. Solid State Chem. 159 (2001) 46.
[9] A. Daidouh, J.L. Martinez, C. Pico, M.L. Veiga, J. Solid State Chem 144 (1999) 169.
[10] F. Menil, J. Phys. Chem. Solids 46 (1985) 763.